ADVANCED ENERGY MATERIALS
www.advenergymat.de

Suppressing Interfacial Dipoles to Minimize Open-Circuit Voltage Loss in Quantum Dot Photovoltaics

Hunhee Lim, Donghun Kim, Min-Jae Choi, Edward H. Sargent, Yeon Sik Jung, and Jin Young Kim**

Quantum-dot (QD) photovoltaics (PVs) offer promise as energy-conversion devices; however, their open-circuit-voltage (V_{OC}) deficit is excessively large. Previous work has identified factors related to the QD active layer that contribute to V_{OC} loss, including sub-bandgap trap states and polydispersity in QD films. This work focuses instead on layer interfaces, and reveals a critical source of V_{OC} loss: electron leakage at the QD/hole-transport layer (HTL) interface. Although large-bandgap organic materials in HTL are potentially suited to minimizing leakage current, dipoles that form at an organic/metal interface impede control over optimal band alignments. To overcome the challenge, a bilayer HTL configuration, which consists of semiconducting alpha-sexithiophene (α-6T) and metallic poly(3,4-ethylenedioxythiphene) polystyrene sulfonate (PEDOT:PSS), is introduced. The introduction of the PEDOT:PSS layer between α-6T and Au electrode suppresses the formation of undesired interfacial dipoles and a Schottky barrier for holes, and the bilayer HTL provides a high electron barrier of 1.35 eV. Using bilayer HTLs enhances the V_{OC} by 74 mV without compromising the J_{SC} compared to conventional MoO_3 control devices, leading to a best power conversion efficiency of 9.2% (>40% improvement relative to relevant controls). Wider applicability of the bilayer strategy is demonstrated by a similar structure based on shallow lowest-unoccupied-molecular-orbital (LUMO) levels.

Photovoltaic (PV) cells containing colloidal quantum dots (QDs) have recently garnered considerable attention owing to their potential as low-cost, large-scale, and air-stable solar-energy-harvesting devices.[1–6] The power conversion efficiencies of QD-PV devices have been dramatically enhanced during the last decade, to the present-day record of over 12%, based on favorable optical properties including facile bandgap (E_g) tunability and wide spectral responses.[7–9] Despite rapid improvements, the performance of QD-PVs is still below the expected level for an active material with this bandgap energy: a large open circuit voltage (V_{OC}) deficit (defined as $V_{SQ} - V_{OC}$, where V_{SQ} is the Shockley–Queisser limit of V_{OC} for a given bandgap) remains a key bottleneck.[5,10] Even state-of-art PbS QD-PVs have V_{OC} deficits in the range of 400–550 mV, which is much larger than that (100–200 mV) of high-efficiency PV cells based on *c*-Si, GaAs, and hybrid perovskites.[11,12]

Previous works identified two QD-related factors responsible for the excessive V_{OC} loss: sub-bandgap trap states and polydispersity in QD films.[5,11–19] A high density of trap states can form in QD materials due to the large surface area and metal-to-chalcogen off-stoichiometry,[10,13,15] and recent works demonstrated that the reduction of the trap states via application of new surface passivation layers can increase the V_{OC} by ≈100 mV.[10,12] Another important factor underlying V_{OC} loss is energy disorder (i.e., bandtail states) within polydisperse QD films.[17] Synthetic modifications in the ligand exchange have recently enabled the realization of increased-monodispersity PbS QD films, and as a result V_{OC} enhancements of up to 90 mV were demonstrated in QD-PVs.[5,16]

Despite recent efforts to tune QD properties, V_{OC} loss is still too large, and there remains therefore a need to develop additional routes to further reduce the loss. Attempts thus far have concentrated mainly on tuning the QD layer only. Comparatively less attention has been paid to the interfaces between constituent layers in the device, although interface optimization is critical to controlling the device leakage current or interfacial recombination, and consequently the V_{OC}. In particular, there have been limited studies on the effect of band engineering at interfaces formed with the hole-transport layer (HTL) on PV performance. At present, MoO_3[20–22] and ethanedithiol (EDT)-passivated QDs (EDT-QDs)[5,6] are the most widely used HTL materials in the QD-PV field. However, these materials provide an insufficiently large energy barrier for electron of 0.2–0.4 eV

H. Lim, Prof. Y. S. Jung
Department of Materials Science and Engineering
Korea Advanced Institute of Science and Technology (KAIST)
291 Daehak-ro, Yuseong-gu, Daejeon 305-701, Republic of Korea
E-mail: ysjung@kaist.ac.kr
Dr. D. Kim
Computational Science Research Center
Korea Institute of Science and Technology (KIST)
Seoul 02792, Republic of Korea
Dr. M.-J. Choi, Prof. E. H. Sargent
Department of Electrical and Computer Engineering
University of Toronto
10 King's College Road, Toronto, Ontario MSS 3G4, Canada
Dr. J. Y. Kim
Center for Hydrogen and Fuel Cell Research
Korea Institute of Science and Technology (KIST)
Seoul 02792, Republic of Korea
E-mail: jinykim@kist.re.kr
The ORCID identification number(s) for the author(s) of this article can be found under https://doi.org/10.1002/aenm.201901938.

DOI: 10.1002/aenm.201901938

(both in our measurements and literature[6,23]), inadequate to block electron leakage.

Large-bandgap organic or conjugated polymer materials are typically characterized by shallow lowest-occupied-molecular-orbital (LUMO) levels, and thus are potentially ideal for HTLs to block electron leakage. These materials, however, often form strong dipole moments at interfaces with metal electrodes in devices,[23–25] which impedes control toward optimal band alignments. In this work, to overcome this challenge, we develop a novel bilayer HTL that consists of semiconducting alpha-sexithiophene (α-6T) and metallic poly(3,4-ethylenedioxythiophene) polystyrene sulfonate (PEDOT:PSS). The introduction of the buffer PEDOT:PSS between α-6T and the Au electrode suppresses the formation of undesired interfacial dipoles and a Schottky barrier for holes, and the bilayer HTL provides a large electron barrier of 1.35 eV. The bilayer HTL enhances the V_{OC} by 74 mV with no J_{SC} sacrifice, compared to control devices, owing to a reduction of the dark leakage current. Moreover, PV devices based on the new HTL are highly stable in air for more than 400 h. We demonstrate that the bilayer HTL strategy is applicable to other small molecules or conjugated polymers that are also characterized by a shallow LUMO. This work reveals that the V_{OC} deficit in QD-PVs is increased by electron leakage at the QD/HTL interface, and suggests a practical solution to minimize the loss.

Today, most advanced QD-PV devices utilize either MoO_3 or EDT-passivated QDs (EDT-QDs) materials as the HTL (**Figure 1**a). For selective and efficient hole extraction, the HTL should satisfy the following three requirements: 1) no barrier for holes, 2) large enough barrier for electrons (desirably >1.0 eV), and 3) high hole mobility ($\mu_h > 10^{-3}$ cm^2 V^{-1} s^{-1}). Although both MoO_3 and EDT-QD satisfy the requirement of the absence of an energy barrier for hole conduction, the other important requirements are not met. For the case of EDT-QD in the HTL, the energy barrier for electrons was measured to be only 0.17 eV, which is not large enough to effectively suppress electron leakage (Figure S1, Supporting Information). Furthermore, the hole mobility of MoO_3 and EDT-QD was estimated to be extremely low, only 7×10^{-5} and 1×10^{-4} cm^2 V^{-1} s^{-1}, respectively.[26,27] These properties raise substantive concerns that conventional HTLs may not function properly, likely leading to considerable loss in V_{OC} and J_{SC}.

It is therefore imperative to identify HTL materials that fulfill the aforementioned three requirements. We focused on small organic molecules and conjugated polymers that are typically characterized by shallow LUMO levels. We built a library of 36 materials, where the energy levels [highest-occupied-molecular-orbital (HOMO) and LUMO levels] and hole mobilities are collected from the literature (Figure 1b,c).[20,21,27–64] To perform sequential screening, we defined quantitative criteria as follows: 1) −5.6 eV < HOMO < −5.1 eV (no barrier for holes), 2) −3.6 eV < LUMO (barrier for electrons >0.75 eV), and 3) $\mu_h > 1.0 \times 10^{-3}$ cm^2 V^{-1} s^{-1}. Materials having a HOMO level shallower than −5.1 eV should also be screened in order to avoid a barrier with an adjacent electrode material (work function of au = −5.1 eV). Based on the screening criteria, we considered the following eight materials as promising HTL materials, in order from shallow to deep LUMO: 5,10,15-tribenzyl-5*H*-diindolo[3,2-*a*:3′,2′-*c*] carbazole (TBDI), 5,10,15-triphenyl-5*H*-diindolo[3,2-*a*:3′,2′-*c*] carbazole (TPDI), α-6T, poly(3-hexylthiophene) (P3HT), poly[[4,8-bis[(2-ethylhexyl)oxy]benzo[1,2-*b*:4,5-*b*′]dithiophene-2,6-diyl][3-fluoro-2-[(2-ethylhexyl)carbonyl]thieno[3,4-*b*] thiophenediyl]] (PTB7), poly(2,6-bis(thiophen-2-yl)-3,5-didecanyldithieno[3,2-b:20 ,30 -d]thiophene)- 3,6-bis(5-bromo-2-thienyl)-2,5-dihydro-2,5-diethylhexylpyrrolo[3,4-c] pyrrole-1,4-dione (PTDTTTDPP), poly[N-9″-hepta-decanyl-2,7-carbazole-alt-5,5-(4′,7′-di-2-thienyl-2′,1′,3′-benzothiadiazole)] (PCDTBT), and poly[2,6-(4,4-bis-(2-ethylhexyl)-4*H*-cyclopenta[2,1-*b*;3,4-*b*′]dithiophene)-alt-4,7(2,1,3-benzothiadiazole)] (PCPDTBT). We mainly focused on using α-6T to demonstrate enhanced PV performance, although we also tested other materials to verify wide applicability of this strategy.

When an organic or conjugated polymer material (α-6T in this case) forms a junction with a metal (Au electrode, in this case) in PV devices, the energy levels at the interface may be substantially shifted due to dipole formation at the organic/metal interface.[23–25] This property could severely limit the potential of these organic/polymer materials in the HTL of QD-PV devices. In our ultraviolet photoelectron spectroscopy (UPS) measurements (Figure S2, Supporting Information), a substantial downward shift (≈0.65 eV) of the vacuum energy level compared to that of noninteractive state (**Figure 2**a) was indeed observed for α-6T when in a direct contact with Au. This results in the formation of Schottky barriers (0.65 eV) for holes at the interface between the Au electrode and α-6T, and thus the hole extraction from α-6T to the Au electrode is undesirably blocked (Figure 2b). The PV devices fail to perform when an Au electrode and α-6T forms a direct junction (Figure S3, Supporting Information).

In order to overcome this critical issue, we investigated the insertion of the metallic polymer PEDOT:PSS between α-6T and Au. We hypothesized that PEDOT:PSS, as a polymer material, would form a much weaker interfacial dipole with α-6T, and at the same time, it is compatible with Au due to its metallic band structure. UPS measurements revealed a negligible shift of energy levels of α-6T after the insertion of the PEDOT:PSS layer (Figure S4, Supporting Information) due to the reduction of the interfacial dipole (Figure 2c). The combined use of PEDOT:PSS (i.e., bilayer HTL) therefore suppresses the formation of the dipole-induced Shottky barrier for holes, and consequently allows facile hole transport from α-6T HTL to the Au electrode.

To clarify the role of the PEDOT:PSS insertion in reducing interfacial dipoles, we performed density-functional-theory (DFT) calculations for several interfacial material systems. It is necessary to compare the energy level shifts at Au/α-6T versus Au/PEDOT:PSS/α-6T system. For the latter case, two interfaces, i.e., PEDOT:PSS/α-6T and Au/PEDOT:PSS, should separately be investigated.

First of all, the interfacial dipoles occurring at each Au/α-6T and PEDOT:PSS/α-6T interface are compared. Since PEDOT:PSS is composed of PEDOT and PSS in different ratios,[65,66] we built separate organic/polymer interfaces with each of PEDOT/α-6T and PSS/α-6T,[67] and also with Au(111)/α-6T for comparison (Figure 2d). Figure 2e shows the interface-induced change of the electrostatic potentials of α-6T for these three interfaces.[22] The vacuum energy levels (flat potential lines in vacuum region) highlight the different

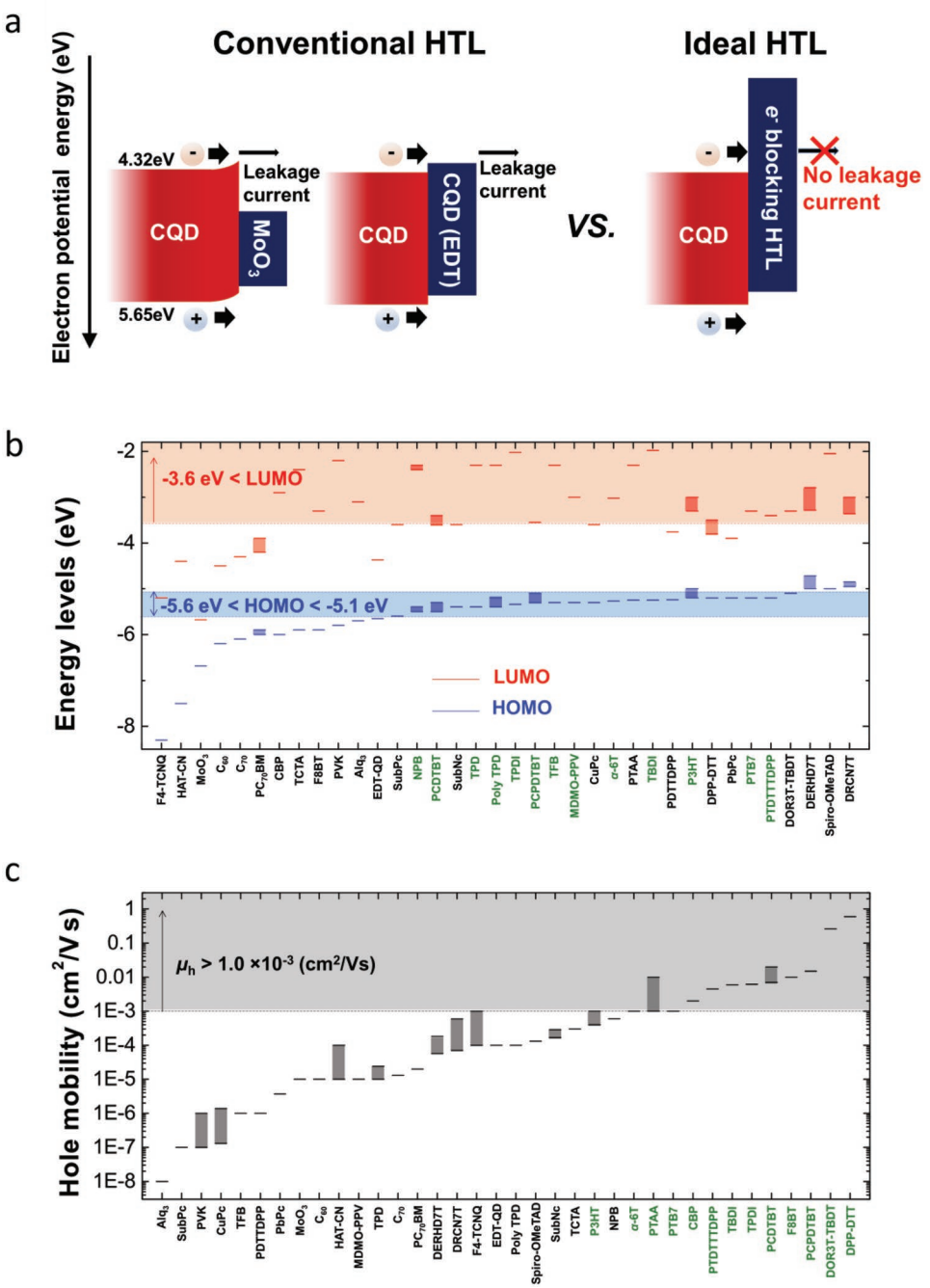

Figure 1. In search of HTL materials toward high-performance QD-PVs. a) Band alignments of conventional versus ideal hole-transport materials for effective charge-carrier collection in QD-PVs, with a particular focus on the barrier formed at the QD/HTL interface. b) LUMO and HOMO levels of candidate HTL materials, collected from the literature.[21,22,25–62] The materials are listed in the order of deep to shallow HOMO levels. The blue and red blocks shaded over the entire materials denote the ideal range for HOMO and LUMO levels, respectively. c) Hole mobility of candidate HTL materials, collected from the literature. The materials are listed in the order of low to high mobility. The gray block shaded over the entire materials denotes the ideal range for hole mobility.

vacuum energy shifts (ΔE_{vac}). A large ΔE_{vac} of around –0.74 eV is observed for Au/α-6T, whereas it is much smaller in magnitude (+0.15 and +0.06 eV) for other PEDOT/α-6T and PSS/α-6T interfaces, respectively. The DFT results of ΔE_{vac} agree well with the UPS measurement results qualitatively. The difference in ΔE_{vac} between Au and PEDOT:PSS originates from the different degree of electron transfer (Figure 2f,i). For Au(111)/α-6T, particularly strong Au-S chemical bonds form, which is favorable to facile electron transfer. For the other two interfaces (PEDOT/α-6T and PSS/α-6T), much weaker van der Waals forces are the primary interactions, which restrict the interfacial charge transfer.

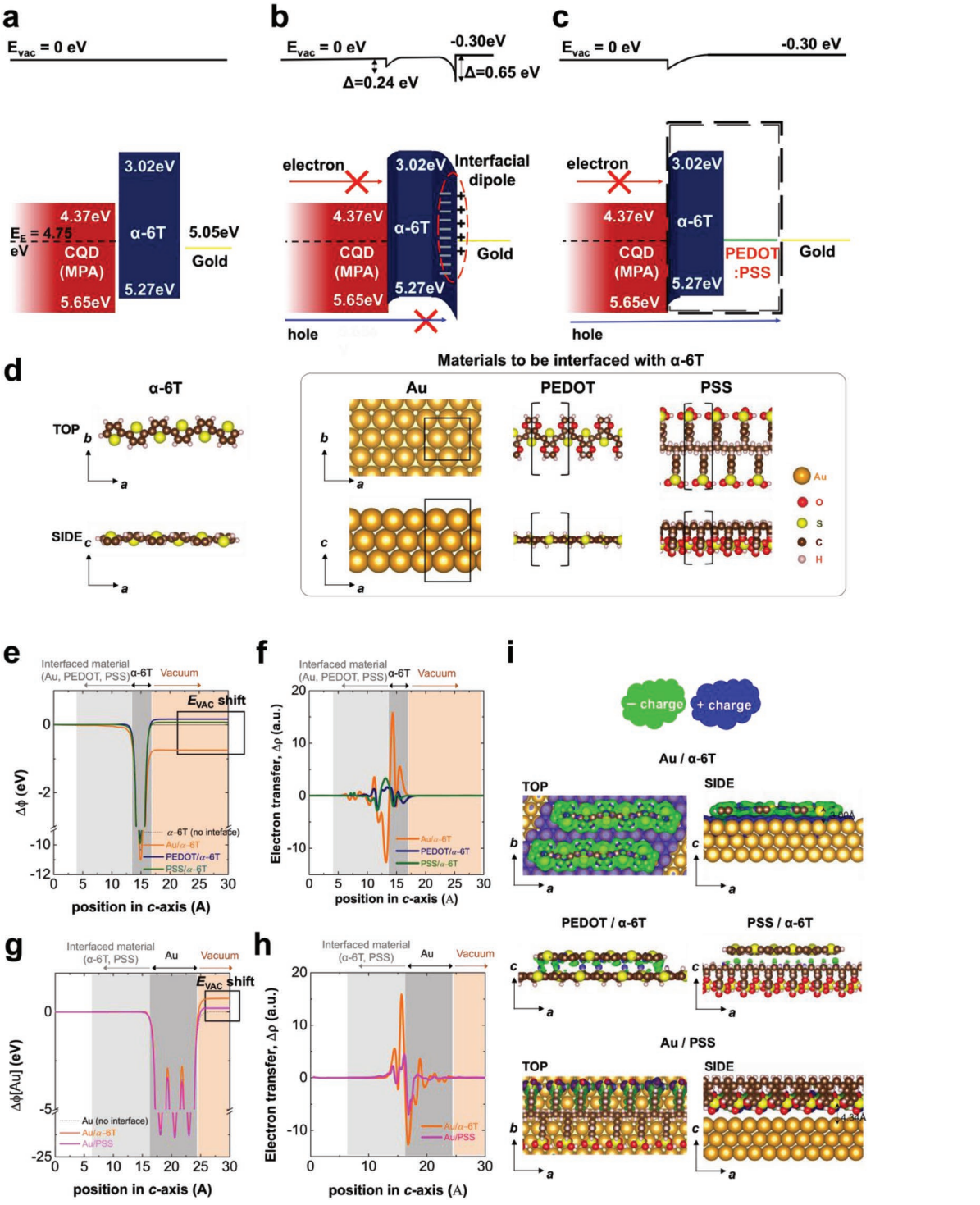

Figure 2. A combined UPS and DFT study to calculate the band structures of QDs, HTL, and electrode in QD-PVs. a–c) Schematics of band diagrams obtained by UPS measurement when each layer is separate a), in contact, when only α-6T is used for the HTL b), in contact, when bilayer materials (α–6T/PEDOT:PSS) are used for the HTL (c), respectively, with a particular focus on interfacial dipoles and related energy-level shift. All numbers in the energy diagrams are calculated with respect to the vacuum energy level of the CQD layer. Note that the dipoles only affect the energy level shifts in the corresponding interfacial regions. d–i) DFT simulation results. d) Each molecular or crystal structure used in DFT simulations of α-6T, Au(111), PEDOT, PSS, e) Interface–induced change in the electrostatic potential of the α–6T system plotted along the *c*-axis (i.e., *ab*-plane averaged), or $\Delta\phi[\alpha\text{-6T}] = \phi_{\text{total}} - \phi_{\text{interfaced-material.}}$ f) Interface-induced electron transfer plotted along the *c*-axis, or $\Delta\rho = \rho_{\text{total}} - [\rho_{\text{interfaced-material}} + \rho_{\alpha\text{-6T}}]$. g) Interface-induced change in the electrostatic potential of the Au(111) system plotted along the *c*-axis, or $\Delta\phi[\text{Au}] = \phi_{\text{total}} - \phi_{\text{interfaced-material.}}$ h) Interface-induced electron transfer plotted along the *c*-axis, or $\Delta\rho = \rho_{\text{total}} - [\rho_{\text{interfaced–material}} + \rho_{\text{Au}}]$. i) 3D visualizations of the charge transfer for four modeled interfaces.

Second, the interfacial dipoles occurring at each Au/α-6T and Au/PEDOT:PSS interface are compared. It is well known that due to vertically phase-segregated PEDOT:PSS, a highly PSS-rich layer forms an interface with the metal electrode (in this case, Au electrode).[65,68]

We thus performed the simulation for the Au/PSS interface with Au/α-6T as a comparison. Figure 2g shows the interface-induced change of the electrostatic potentials of Au for these two interfaces. The results reveal that a much weaker dipole forms at the Au/PSS interface (ΔE_{vac} of 0.19 eV in the highlighted box in Figure 2g) than the Au/α-6T case (0.74 eV), which qualitatively agrees with UPS measurements (Figure S2, Supporting Information). This is because the sulfonate (SO_3^-) geometry in PSS and gold bonds is much weaker bonding than direct Au-S bonds. The calculated Au-S distance is 4.34 Å at the Au/PSS interface, which is much larger than 3.00 Å in the Au/α-6T case (Figure 2h,i). Overall, our simulations support the experimental results that the insertion of PEDOT:PSS weakens the dipoles on both sides with Au and α-6T, and demonstrate how PEDOT:PSS can suppress the formation of the undesired Schottky barrier for holes.

The incorporation of the new bilayer HTL (α-6T/PEDOT:PSS) substantially improved the performance of QD-PVs, compared to the control devices based on MoO_3 HTL (**Figure 3**a and **Table 1**). The *J–V* curves in Figure 3a reveal that the use of the bilayer HTL improved the V_{OC} by 74 mV and J_{SC} by 3.5 mA cm^{-2}, leading to a best power conversion efficiency (PCE) of 9.2%. The PCE enhancement is a general observation, confirmed from more than 30 device samples (Figure 3b). Importantly, it should be noted that enhancements of the performance factors (V_{OC}, J_{SC}, fill factor) are also observed when EDT-QDs are used as the control HTL material, instead of MoO_3 (Figure S5, Supporting Information).

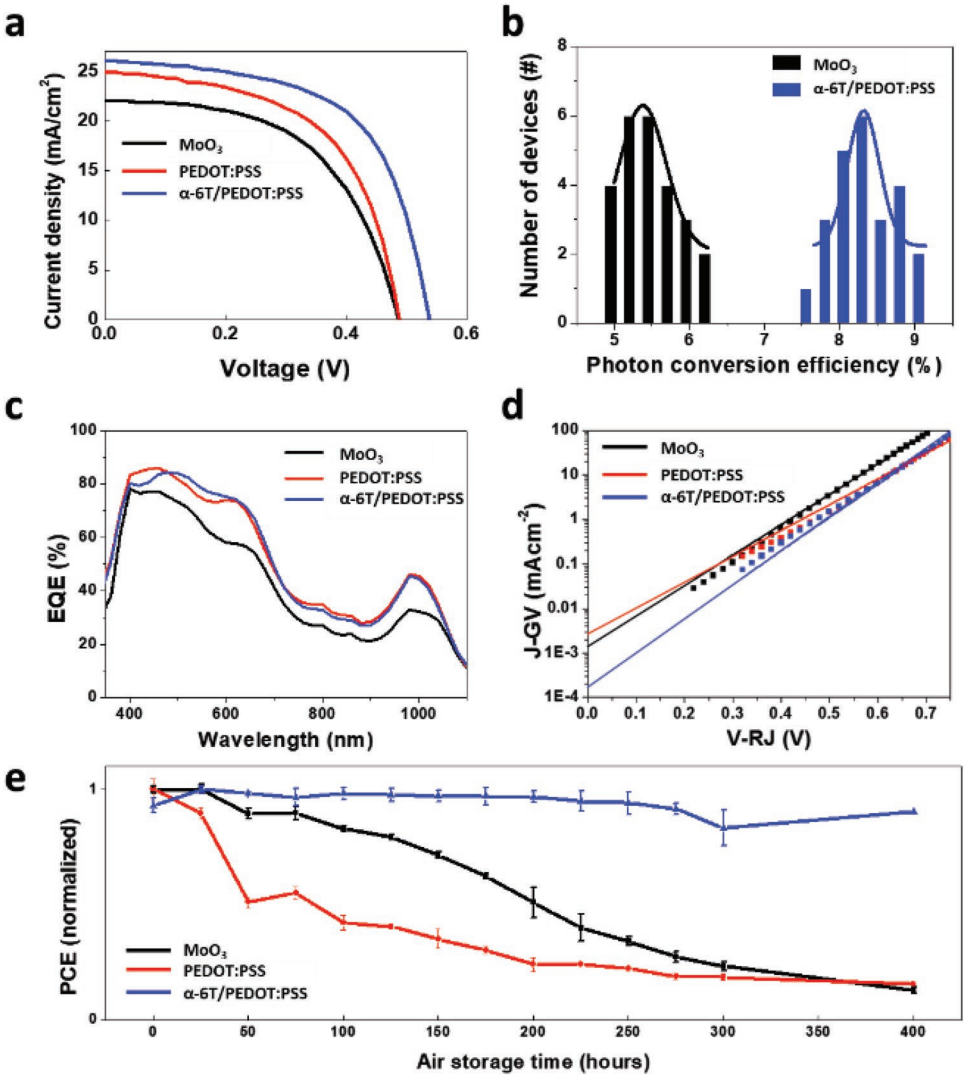

Figure 3. QD-PV performance, characterizations, and air stability. a) *J–V* curves of the devices with different HTL materials (MoO_3, PEDOT:PSS alone, and α–6T/PEDOT:PSS). b) A histogram highlighting the PCE distributions of PV devices obtained from numerous experimental tests. c) External quantum efficiency (EQE) of the PV devices. d) *J*-GV versus *V*-RJ graphs of the PV devices to obtain dark leakage current (J_0, the intercept at *y*-axis), where *G* and *R* refer to conductance and resistance, respectively. e) Stability tests of the PV devices stored in air for 400 h.

Table 1. Statistical performance data of QD-PV devices with different HTL materials.

	[a]V_{OC} [V]	[a]J_{SC} [mA cm^{-2}]	[a]Fill factor [%]	[a]PCE (%)	[b]J_0 (mA cm^{-2})
MoO_3	0.50 ± 0.02 (0.52)	20.7 ± 1.2 (21.3)	55.9 ± 4.5 (58.6)	5.8 ± 0.4 (6.4)	$1.5 \pm 0.3 \times 10^{-3}$
PEDOT:PSS	0.52 ± 0.02 (0.53)	24.2 ± 1.3 (23.6)	56.3 ± 2.8 (60.5)	7.0 ± 0.3 (7.6)	$1.3 \pm 0.2 \times 10^{-3}$
α–6T/PEDOT:PSS	0.57 ± 0.02 (0.57)	24.2 ± 1.5 (25.6)	60.0 ± 2.4 (62.7)	8.3 ± 0.5 (9.2)	$2.7 \pm 0.2 \times 10^{-4}$

[a]Each PV performance parameter is averaged over 30 samples. The numbers in the parenthesis are the values of the best performing device; [b]J_0 is averaged from 5 samples.

We also compare the performance of the bilayer HTL structure with that of single-layered HTLs, i.e., PEDOT:PSS or α-6T layer alone. Using single-layer PEDOT:PSS with a higher hole mobility improved only the J_{SC} (no V_{OC} enhancement). This indicates that the observed J_{SC} enhancement for the bilayer HTLs case is mainly due to the increased hole mobiliity of the PEDOT:PSS layer. The external quantum efficiency (EQE) results presented in Figure 3c also clarify the origins of the J_{SC} enhancements. The PEDOT:PSS and α-6T/PEDOT:PSS exhibit larger EQE values than the MoO_3 case over the entire wavelength range. Second, simply replacing MoO_3 with α-6T results in unacceptably inefficient device performance (PCE ≈ 0.24%, Figure S3, Supporting Information). This result can be explained by the energy band diagram (Figure 2b) determined from the UPS measurement data. The diagram shows that hole extraction from QDs is undesirably blocked due to the substantial downward shift of the vacuum energy level of α-6T. These comparisons of device performance confirm that the combined use of α-6T and PEDOT:PSS in HTL is indeed beneficial.

To investigate any connection between the V_{OC} improvement in the bilayer HTL and the existence of electron leakage, we acquired dark *J*–*V* characteristics. V_{OC} is inversely related to the dark current density (J_0) as follows

$$V_{OC} = \frac{nkT}{q} \ln\left(\frac{J_{SC}}{J_0}\right) \quad (1)$$

where *n* is the diode ideality factor, *k* is the Boltzmann constant, *T* is the temperature, *q* is the electric charge constant. The total dark diode current can be expressed

$$J = J_0 \exp\left[\frac{q}{nkT}(V - RJ)\right] + GV \quad (2)$$

where *R* is the series resistance and *G* is the shunt conductance. In the graph of *J*-GV versus *V*-RJ in Figure 3d, J_0 was determined as the value of the *y*-intercept (at *V*-RJ = 0). Devices using MoO_3 or PEDOT:PSS alone for HTL produced a dark current density (J_0) of around 1.2×10^{-3}–1.5×10^{-3} mA cm^{-2}. On the other hand, the device using the bilayer HTL of α-6T/PEDOT:PSS exhibited notably reduced (about 1/5) leakage current density (2.7×10^{-4} mA cm^{-2}).

The quantitative impact of J_0 reduction on V_{OC} enhancement is assessed using Equation (1). Based on the measured J_0 and J_{SC} values (Table 1), the term $n\ln(J_{SC}/J_0)$ for the bilayer HTL device was estimated to be 8.1% and 16.1% larger than those of the cases of PEDOT:PSS and MoO_3 alone, respectively. These values agree well with the V_{OC} enhancements in the device characterization results, improvements of 10.9% (compared to PEDOT:PSS alone) and 14.9% (compared to MoO_3 alone). These quantitative comparisons indicate that the observed V_{OC} improvements can be ascribed to the reduced leakage current in dark, enabled by the introduction of the substantial electron blocking barrier of 1.35 eV by the new bilayer HTL. These results support that electron leakage in the dark at the QD/HTL interface is an important V_{OC} loss mechanism.

Another beneficial result of the bilayer HTL is long-term air stability of PV devices. The devices with three different HTLs (i.e., MoO_3, PEDOT:PSS, and α-6T/PEDOT:PSS) were stored in air for 400 h, and the PV device performance was measured on a daily basis. Figure 3e shows the history of PV performance over time. The new bilayer HTL of α-6T/PEDOT:PSS substantially improved the PV device stability in air, compared to the case of MoO_3 or PEDOT:PSS alone. For the new bilayer HTL, the average PCE remained constant even following 400 h air storage, while a substantial drop in the PCE was observed for the other cases (both PCEs dropped to below 15% of initial performance after 400 h). The poor air stability of the MoO_3 device is consistent with previous studies, and the degradation can be attributed to the MoO_3 being highly vulnerable to oxidation.[69] The use of PEDOT:PSS is also known to degrade the devices due to its acidic and hygroscopic nature.[70,71] In other words, the PbS QDs in contact with PEDOT:PSS will likely be susceptible to oxidation. For the α-6T/PEDOT:PSS case, however, the insertion of α-6T layer blocks the direct contact between the QDs and PEDOT:PSS layer, markedly improving air stability.

To demonstrate the wide applicability of the bilayer HTL strategy, we also considered other materials (TBDI, TPDI, P3HT, PTB7, PTDTTTDPP, PCDTBT, and PCPDTBT) chosen via the aforementioned screening process (Figure 1b,c). We tested QD-PV devices with two polymer HTL materials, i.e., P3HT and PCPDTBT, both of which satisfy the requirements of HOMO/LUMO levels and hole mobility. Similar to the α-6T case, the PV devices with P3HT or PCPDTBT alone in HTL do not function properly, likely due to the dipole-induced Schottky barrier for holes (**Figure 4**a). To prevent the substantial interfacial dipole between these polymers and Au electrode, PEDOT:PSS is also inserted in each case. Therefore, additional bilayer HTL structures, P3HT/PEDOT:PSS and PCPDTBT/PEDOT:PSS, are tested. Using bilayer HTL leads to the efficient PV functioning for all cases (Figure 4a). It is important to note that V_{OC} enhancements are observed for these two HTLs (by 66 mV for the former and by 33 mV for the latter), compared to the control device of PEDOT:PSS alone, with no compromise to J_{SC} for all.

In Figure 4b, V_{OC} enhancements are shown as a function of the electron blocking barrier at the QD/HTL junction for each small molecule or conjugated polymer case (α-6T, P3HT,

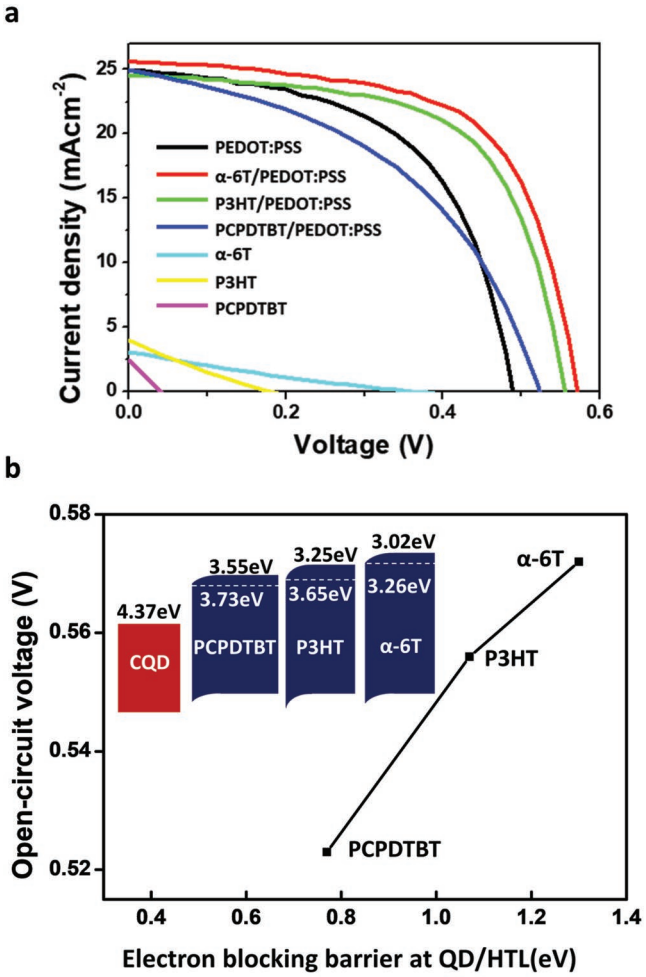

Figure 4. Extended applicability of the bilayer HTL strategy for V_{OC} enhancement. a) P3HT and PCPDTBT are further selected for these tests, as they satisfy the requirements of an ideal HTL (Figure 1). *J–V* characteristics of each HTL material are shown and compared. b) V_{OC} enhancements are plotted as a function of the electron blocking barrier at each QD/HTL junction.

and PCPDTBT) in the bilayer HTL. The electron blocking barrier at the QD/HTL junction can be estimated by the difference between the LUMO level of the HTL material and the CBM level of the QD layer, i.e., Δ = LUMO (HTL) − CBM (QD). A positive correlation between Δ and V_{OC} enhancement is observed in Figure 4b, supporting that the V_{OC} deficit in QD-PV is quantitatively impacted by electron leakage at the QD/HTL interface. This result suggests that small molecules or conjugated polymers characterized by shallow LUMO levels are more effective in reducing the electron leakage, and thus should be prioritized in the design of the bilayer HTL. Overall, the improvements in V_{OC}, J_{SC}, and air stability support that our work provides a properly designed HTL scheme to enhance the competitiveness of QD-PVs.

In summary, this study reveals that electron leakage at the interface between QDs and the HTL causes excessive V_{OC} loss in conventional QD-PVs. Owing to their shallow LUMO levels and high hole mobilities, some conjugated small molecules including α-6T are potentially suited for minimizing the leakage currents; however, interfacial dipoles formed at the metal-organic semiconductor junction produce a Schottky barriers for holes and hinder the PV functioning. In our case, the dipole formed at the interface between α-6T and the Au electrode forms a Schottky barrier of 0.65 eV, which impedes efficient hole extraction. To overcome this issue, we developed bilayer HTLs wherein a conducting polymer (PEDOT:PSS) buffer layer was introduced between α-6T and the Au electrode, which in turn substantially relieves the interfacial dipoles. We confirm that our bilayer HTL comprising sequential α-6T and PEDOT:PSS layers effectively suppress the undesired Schottky barrier for holes while providing a high electron blocking barrier of 1.35 eV.

The bilayer HTL experimentally improved the V_{OC} by 74 mV in QD-PVs (without compromising J_{SC}), compared to the reference MoO_3 HTL case. This strategy is compatible with other previous achievements based on QD ligand engineering (e.g., EDT-passivated QDs as the reference HTL). We confirm that the sufficiently large electron blocking barrier (≈1.5 eV) of the bilayer HTL reduces the dark leakage current by a factor of 5, which is quantitatively well correlated with the V_{OC} enhancements observed in the device characterization. Additionally, the new HTL offers considerably improved PV device stability in air, reaching more than 400 h. Few studies have achieved simultaneous improvements in V_{OC}, J_{SC}, and air stability without a trade-off, and this is a unique strength of the new HTL scheme. By confirming analogous effects in V_{OC} improvements, we further demonstrated that our bilayer HTL strategy is widely applicable to other conjugated polymers and small molecules characterized by shallow LUMO levels.

Experimental Section

Density-Functional-Theory Calculations: All the calculations were performed using the Vienna Ab Initio Simulation Packages (VASP)[72] with an energy cutoff of 480 eV. The projector-augmented-wave (PAW) method was adopted to describe the potential of the ionic cores.[73] The generalized gradient approximation of revised Perdew–Burke–Ernzerhof (rPBE) was employed for the exchange and correlation functional.[74] van der Waals corrections were included. For Au slab system, (111) surface was chosen since it was known as the most stable low-index surface. For the Au/α-6T system, a 6 × 1 supercell of Au (111) unit (35.8 Å in *a*-axis) was built to make an interface with the α-6T molecule (i.e., Au/α-6T), as shown in Figure 2i. The Monkhorst–Pack *k*-point sampling of 1 × 3 × 1 was used. For the Au/PSS system, a 5 × 2 supercell of Au (111) unit (29.8 Å in *a*-axis) was built to make an interface with the PSS polymer (i.e., Au/PSS). The Monkhorst–Pack k-point sampling of 2 × 2 × 1 was used. For both Au/α-6T and Au/PSS systems, each Au (111) slab consisted of three single layers, where the bottom layer was not allowed to relax. That is, α-6T, PSS, and the top two layers of the Au slab were fully relaxed. For the other two interfacial systems, or α-6T/PEDOT and α-6T/PSS, various initial geometries and relative orientations of α-6T/PEDOT and α-6T/PSS interfaces were tested, and the geometry having minimum energy was selected and shown in Figure 2i. For these two systems, the Monkhorst–Pack *k*-point sampling of 1 × 1 × 1 was used. The geometry relaxation was accomplished using the conjugate gradient method until the maximum forces acting on each atom become less than 0.02 eV Å^{-1}. Dipole corrections were included to remove the spurious electrostatic interactions between neighboring supercells.

Materials: Lead(II) oxide powder (PbO) (99%), 1-octadecene (ODE) (technical grade 90%), oleic acid (OA) (technical grade 90%), oleylamine (OLA) (technical grade 70%), hexamethyldisilathiane

($(TMS)_2S$) (synthesis grade), tetrabutylammonium iodide (TBAI) (99%), mercaptopropionic acid (MPA), and alpha-sexithiophene (α-6T) were purchased from Sigma-Aldrich and poly (3,4-ethylenedioxythiophene)-poly(styrenesulfonate) (PEDOT:PSS) was purchased from Heraeus.

Synthesis of PbS Quantum Dots: The synthesis method was adapted from the literature.[75] Lead oxide (0.9 g) was dissolved in ODE (25 mL) with OA (2.7 mL). The solution was degassed and stirred overnight at 100 °C. Afterward, the lead precursor solution was degassed with nitrogen and the temperature was increased to 120 °C. The sulfur precursor was prepared by dissolving hexamethyldisilathiane (360 µL) in ODE (10 mL). The lead precursor solution was vigorously stirred while the sulfur precursor solution was swiftly injected and cooled to 35 °C. The QDs were extracted and purified by acetone followed by centrifugation. The QDs were re-dissolved in toluene and washed three times by acetone and methanol followed by centrifugation. Finally, the QDs were dispersed in octane with concentration of 50 mg mL^{-1} and stored in a glovebox.

Synthesis of ZnO Nanoparticles: The synthesis method was adapted from the literature.[6] Zinc acetate (2.95 g) was dissolved in methanol (125 mL) at 60 °C. Another solution of potassium hydroxide (1.48 g) was dissolved in methanol (65 mL). The solution with potassium hydroxide was slowly added to the zinc acetate solution and the injection was terminated after 10 min. The solution was continuously stirred at 60 °C for 2.5 h. Afterward, the solution was extracted by centrifugation and the precipitants were washed twice by methanol followed by centrifugation. The precipitants were kept wet with methanol and dissolved in chloroform (10 mL). The final solution was filtered and kept in a refrigerator.

Device Fabrication: The ITO substrate was cleaned with solvents and treated with UV ozone. The ZnO solution was spin-coated to fabricate a 60 nm thick film. PbS QD films were deposited by layer-by-layer spin coating. 15 µL of PbS QD solution was spin coated onto the substrate at 2500 rpm for 15 s. The PbS QD film was then soaked by TBAI solution (10 mg mL^{-1} in methanol) for 30 s and washed with methanol three times. The TBAI-QD film fabrication process was repeated eight times (final thickness = 180 nm). For MPA-QD layers, a MPA solution (10 mg mL^{-1} in methanol) was used and the process was repeated two times (final thickness = 40 nm). MoO_3 (20 nm), α-6T (50 nm), and a gold/silver (40 nm/180 nm) electrode were deposited by a thermal evaporator at a pressure below 1×10^{-5} torr. The PEDOT:PSS solution (purchased solution was diluted by methanol by 33% in volume fraction) was spin coated at 5000 rpm for 60 s.

Device Characterization: A UV–vis spectrophotometer (Mecasys, Optizen POP, Korea) was used to obtain UV–vis absorption spectra of PbS QDs. A scanning electron microscope (FE-SEM, Hitachi, S-4800) was used to observe the cross-section of the QD film. A Keithley 2450 source meter was used to obtain the current-voltage characteristics. *J–V* sweeps were performed in a N_2 filled glove box. A 150 W Xe lamp with an AM 1.5G filter (LS-150-Xe, Abet Technologies) was used to illuminate the device.

Supporting Information

Supporting Information is available from the Wiley Online Library or from the author.

Acknowledgements

H.L. and D.K. contributed equally to this work. This work was supported by KIST Institutional Program (2E28271) and Creative Materials Discovery Program through the National Research Foundation of Korea (NRF-2016M3D1A1021140 and NRF-2016M3D1A1900035) and the Hydrogen Energy Innovation Technology Development Program of the National Research Foundation of Korea (NRF) funded by the Korean government (Ministry of Science and ICT (MSIT)) (No. 2019M3E6A1063674).

Conflict of Interest

The authors declare no conflict of interest.

Keywords

band engineering, hole transport layers, interfacial dipole, quantum dot solar cells

Received: June 17, 2019
Revised: September 11, 2019
Published online:

[1] S. A. McDonald, G. Konstantatos, S. Zhang, P. W. Cyr, E. J. D. Klem, L. Levina, E. H. Sargent, *Nat. Mater.* **2005**, *4*, 138.
[2] S. Coe-Sullivan, J. S. Steckel, W. K. Woo, M. G. Bawendi, V. Bulovic, *Adv. Funct. Mater.* **2005**, *15*, 1117.
[3] J. M. Caruge, J. E. Halpert, V. Wood, V. Buloví, M. G. Bawendi, *Nat. Photonics* **2008**, *2*, 247.
[4] I. J. Kramer, E. H. Sargent, *Chem. Rev.* **2014**, *114*, 863.
[5] M. Liu, O. Voznyy, R. Sabatini, F. P. García De Arquer, R. Munir, A. H. Balawi, X. Lan, F. Fan, G. Walters, A. R. Kirmani, S. Hoogland, F. Laquai, A. Amassian, E. H. Sargent, *Nat. Mater.* **2017**, *16*, 258.
[6] C. H. M. Chuang, P. R. Brown, V. Bulović, M. G. Bawendi, *Nat. Mater.* **2014**, *13*, 796.
[7] A. J. Labelle, S. M. Thon, S. Masala, M. M. Adachi, H. Dong, M. Farahani, A. H. Ip, A. Fratalocchi, E. H. Sargent, *Nano Lett.* **2015**, *15*, 1101.
[8] R. A. Taylor, K. Ramasamy, *SPR Nanosci.* **2017**, *4*, 142.
[9] M. Graetzel, R. A. J. Janssen, D. B. Mitzi, E. H. Sargent, *Nature* **2012**, *488*, 304.
[10] S. Pradhan, A. Stavrinadis, S. Gupta, S. Christodoulou, G. Konstantatos, *ACS Energy Lett.* **2017**, *2*, 1444.
[11] C. H. M. Chuang, A. Maurano, R. E. Brandt, G. W. Hwang, J. Jean, T. Buonassisi, V. Bulović, M. G. Bawendi, *Nano Lett.* **2015**, *15*, 3286.
[12] S. Pradhan, A. Stavrinadis, S. Gupta, Y. Bi, F. Di Stasio, G. Konstantatos, *Small* **2017**, *13*, 1700598.
[13] D. Kim, D. H. Kim, J. H. Lee, J. C. Grossman, *Phys. Rev. Lett.* **2013**, *110*, 196802.
[14] D. K. Ko, A. Maurano, S. K. Suh, D. Kim, G. W. Hwang, J. C. Grossman, V. Bulović, M. G. Bawendi, *ACS Nano* **2016**, *10*, 3382.
[15] G. W. Hwang, D. Kim, J. M. Cordero, M. W. B. Wilson, C. H. M. Chuang, J. C. Grossman, M. G. Bawendi, *Adv. Mater.* **2015**, *27*, 4481.
[16] J. W. Jo, Y. Kim, J. Choi, F. P. G. de Arquer, G. Walters, B. Sun, O. Ouellette, J. Kim, A. H. Proppe, R. Quintero-Bermudez, J. Fan, J. Xu, C. S. Tan, O. Voznyy, E. H. Sargent, *Adv. Mater.* **2017**, *29*, 1.
[17] D. Zhitomirsky, I. J. Kramer, A. J. Labelle, A. Fischer, R. Debnath, J. Pan, O. M. Bakr, E. H. Sargent, *Nano Lett.* **2012**, *12*, 1007.
[18] Y. Liu, D. Kim, O. P. Morris, D. Zhitomirsky, J. C. Grossman, *ACS Nano* **2018**, *12*, 2838.
[19] O. Voznyy, L. Levina, F. Fan, G. Walters, J. Z. Fan, A. Kiani, A. H. Ip, S. M. Thon, A. H. Proppe, M. Liu, E. H. Sargent, *Nano Lett.* **2017**, *17*, 7191.
[20] J. Gao, C. L. Perkins, J. M. Luther, M. C. Hanna, H. Y. Chen, O. E. Semonin, A. J. Nozik, R. J. Ellingson, M. C. Beard, *Nano Lett.* **2011**, *11*, 3263.

[21] P. R. Brown, R. R. Lunt, N. Zhao, T. P. Osedach, D. D. Wanger, L. Y. Chang, M. G. Bawendi, V. Bulović, *Nano Lett.* **2011**, *11*, 2955.
[22] P. R. Brown, D. Kim, R. R. Lunt, N. Zhao, M. G. Bawendi, J. C. Grossman, V. Bulović, *ACS Nano* **2014**, *8*, 5863.
[23] H. Ishii, H. Oji, E. Ito, N. Hayashi, D. Yoshimura, K. Seki, *J. Lumin.* **2000**, *87*, 61.
[24] M. Grobosch, M. Knupfer, *Org. Electron.* **2007**, *8*, 625.
[25] K. Antoine, K. Norbert, G. Weiying, *J. Polym. Sci., Part B: Polym. Phys.* **2003**, *41*, 2529.
[26] E. J. D. Klem, H. Shukla, S. Hinds, D. D. MacNeil, L. Levina, E. H. Sargent, *Appl. Phys. Lett.* **2008**, *92*, 1.
[27] M. Vasilopoulou, A. Soultati, P. Argitis, T. Stergiopoulos, D. Davazoglou, *J. Phys. Chem. Lett.* **2014**, *5*, 1871.
[28] L. S. Liao, W. K. Slusarek, T. K. Hatwar, M. L. Ricks, D. L. Comfort, *Adv. Mater.* **2008**, *20*, 324.
[29] M. P. Patankar, K. Joshi, K. L. Narasimhan, arXiv:1312.0223, **2008**, 1.
[30] Y. Wang, Q. Liang, J. Huang, D. Ma, Y. Jiao, *RSC Adv.* **2017**, *7*, 28494.
[31] A. Opitz, M. Bronner, W. Brütting, *J. Phys.: Conf. Ser.* **2008**, *100*, 082043.
[32] K. Tokunaga, *Hydrogenation of Fulerene C60: Material Design of Organic Semiconductors by Computation*, IntechOpen, London **2012**.
[33] T. Zhuang, X. F. Wang, T. Sano, Z. Hong, G. Li, Y. Yang, J. Kido, *Appl. Phys. Lett.* **2014**, *105*, 093301.
[34] Q. Zhang, B. Kan, F. Liu, G. Long, X. Wan, X. Chen, Y. Zuo, W. Ni, H. Zhang, M. Li, Z. Hu, F. Huang, Y. Cao, Z. Liang, M. Zhang, T. P. Russell, Y. Chen, *Nat. Photonics* **2014**, *9*, 35.
[35] M. Stolterfoht, S. Shoaee, A. Armin, H. Jin, I. Kassal, W. Jiang, P. Burn, P. Meredith, *Adv. Energy Mater.* **2017**, *7*, 1601379.
[36] T. D. Anthopoulos, D. M. De Leeuw, E. Cantatore, P. Van't Hof, J. Alma, J. C. Hummelen, *J. Appl. Phys.* **2005**, *98*, 054503.
[37] B. Ebenhoch, S. A. J. Thomson, K. Genevičius, G. Juška, I. D. W. Samuel, *Org. Electron.* **2015**, *22*, 62.
[38] K. Cnops, B. P. Rand, D. Cheyns, B. Verreet, M. A. Empl, P. Heremans, *Nat. Commun.* **2014**, *5*, 1.
[39] C. Xiang, W. Koo, F. So, H. Sasabe, J. Kido, *Light: Sci. Appl.* **2013**, *2*, 1.
[40] M. Nikolka, I. Nasrallah, B. Rose, M. K. Ravva, K. Broch, A. Sadhanala, D. Harkin, J. Charmet, M. Hurhangee, A. Brown, S. Illig, P. Too, J. Jongman, I. McCulloch, J. L. Bredas, H. Sirringhaus, *Nat. Mater.* **2017**, *16*, 356.
[41] S. Ambrozevich, M. Van Der Auweraer, D. Dirin, M. Parshin, R. Vasil'Ev, A. Vitukhnovsky, *J. Russ. Laser Res.* **2008**, *29*, 526.
[42] H. H. Fong, S. K. So, *J. Appl. Phys.* **2006**, *100*, 094502.
[43] T. D. Hoanh, Y. H. Im, D.-E. Kim, Y.-S. Kwon, B.-J. Lee, *J. Nanomater.* **2012**, *2012*, 451306.
[44] N. Mendil, M. Daoudi, Z. Berkai, A. Belghachi, *J. Phys.: Conf. Ser.* **2014**, *647*, 012057.
[45] C. Kulshreshtha, G. W. Kim, R. Lampande, D. H. Huh, M. Chae, J. H. Kwon, *J. Mater. Chem. A* **2013**, *1*, 4077.
[46] H. Kim, K. G. Lim, T. W. Lee, *Energy Environ. Sci.* **2016**, *9*, 12.
[47] J. Hou, X. Guo, in *Organic Solar Cells: Materials Device Physics* (Ed: W. C. H. Choy), Springer London, London, **2013**, pp. 17–42.
[48] S. Cho, J. H. Seo, S. H. Park, S. Beaupré, M. Leclerc, A. J. Heeger, *Adv. Mater.* **2010**, *22*, 1253.
[49] S. Cheylan, J. Puigdollers, H. J. Bolink, E. Coronado, C. Voz, R. Alcubilla, G. Badenes, *J. Appl. Phys.* **2008**, *103*, 10.
[50] M. Morana, M. Wegscheider, A. Bonanni, N. Kopidakis, S. Shaheen, M. Scharber, Z. Zhu, D. Waller, R. Gaudiana, C. Brabec, *Adv. Funct. Mater.* **2008**, *18*, 1757.
[51] M. D. Ho, D. Kim, N. Kim, S. M. Cho, H. Chae, *ACS Appl. Mater. Interfaces* **2013**, *5*, 12369.
[52] A. W. Hains, T. J. Marks, *Appl. Phys. Lett.* **2008**, *92*, 023504.
[53] M Geoghegan, G. Hadziioannou, *Polymer Electronics*, Oxford University Press, Oxford **2013**.
[54] C. A. Amorim, M. R. Cavallari, G. Santos, F. J. Fonseca, A. M. Andrade, S. Mergulhão, *J. Non-Cryst. Solids* **2012**, *358*, 484.
[55] F. Huang, Y. Peng, K. Xu, W. Lv, S. Xu, Y. Wang, Y. Tang, Y. Wei, Y. Yang, G. Liu, *J. Phys. D. Appl. Phys.* **2017**, *50*, 205106.
[56] F. Zhao, X. Luo, J. Liu, L. Du, W. L. Lv, L. Sun, Y. Li, Y. Wang, Y. Peng, *J. Mater. Chem. C* **2015**, *4*, 815.
[57] M. A. Loi, E. D. A. Como, F. Dinelli, M. Murgia, R. Zamboni, F. Biscarini, M. Muccini, *Nat. Mater.* **2005**, *4*, 81.
[58] A. V. Patil, W. H. Lee, K. Kim, H. Park, I. N. Kang, S. H. Lee, *Polym. Chem.* **2011**, *2*, 2907.
[59] T.-W. Lee, K.-G. Lim, D.-H. Kim, *Electron. Mater. Lett.* **2010**, *6*, 41.
[60] K. Yang, Y. Wang, A. Jain, L. Samulson, J. Kumar, *J. Macromol. Sci., Part A: Pure Appl.Chem.* **2007**, *44*, 1261.
[61] H. Wei, L. Scudiero, H. Eilers, *Appl. Surf. Sci.* **2009**, *255*, 8593.
[62] F. Yang, C. Li, J. Zhang, G. Feng, Z. Wei, W. Li, *Org. Electron.* **2016**, *37*, 366.
[63] Y. Liu, Q. Chen, H. S. Duan, H. Zhou, Y. Yang, H. Chen, S. Luo, T. Bin Song, L. Dou, Z. Hong, Y. Yang, *J. Mater. Chem. A* **2015**, *3*, 11940.
[64] F. Ullah, H. Chen, C. Z. Li, *Chinese Chem. Lett.* **2017**, *28*, 503.
[65] D. H. Kim, K. G. Lim, J. H. Park, T. W. Lee, *ChemSusChem* **2012**, *5*, 2053.
[66] A. Lenz, H. Kariis, A. Pohl, P. Persson, L. Ojamäe, *Chem. Phys.* **2011**, *384*, 44.
[67] Y. Kanai, J. C. Grossman, *Nano Lett.* **2007**, *7*, 1967.
[68] K. Anil, W. Milne, J. Jang, *Sol. Energy Mater. Sol. Cells* **2015**, *132*, 623.
[69] M. T. Greiner, M. G. Helander, W. M. Tang, Z. Bin Wang, J. Qiu, Z. H. Lu, *Nat. Mater.* **2012**, *11*, 76.
[70] M. Jørgensen, K. Norrman, F. C. Krebs, *Sol. Energy Mater. Sol. Cells* **2008**, *92*, 686.
[71] K. Norrman, M. V. Madsen, S. A. Gevorgyan, F. C. Krebs, *J. Am. Chem. Soc.* **2010**, *132*, 16883.
[72] J. F. G. Kresse, *Phys. Rev. B - Condens. Matter Mater. Phys.* **1996**, *54*, 169.
[73] D. G. Kresse, *Joubert, Phys. Rev. B - Condens. Matter Mater. Phys.* **1999**, *59*, 1758.
[74] B. Hammer, L. B. Hansen, J. K. Nørskov, *Phys. Rev. B - Condens. Matter Mater. Phys.* **1999**, *59*, 7413.
[75] Y. Cheng, E. S. Arinze, N. Palmquist, S. M. Thon, *Nanophotonics* **2016**, *5*, 31.

